CHAPTER

7

Surface Electromagnetic Waves on Structured Perfectly Conducting Surfaces

Alexei A. Maradudin
Research Professor, Physics and Astronomy School of Physical Sciences, University of California, Irvine, CA, USA

A planar interface between a dielectric medium, e.g. vacuum, and a perfect conductor does not support a surface electromagnetic wave. This is easily seen.

Let us consider a system consisting of vacuum in the region $x_3 > 0$. We assume that a p-polarized electromagnetic wave of frequency ω is propagating in the x_1 direction along the planar surface of a semi-infinite perfect conductor that occupies the region $x_3 < 0$. The magnetic field in the vacuum region $x_3 > 0$, $\mathbf{H}(\mathbf{x}; t) = (0, H_2(x_1, x_3|\omega), 0)\ \exp(-i\omega t)$, had only a single nonzero component. The amplitude $H_2(x_1, x_3|\omega)$ satisfies the equation

$$\left(\frac{\partial^2}{\partial x_1^2} + \frac{\partial^2}{\partial x_3^2} + \frac{\omega^2}{c^2}\right) H_2(x_1, x_3|\omega) = 0, \tag{7.1}$$

together with the boundary condition

$$\frac{\partial}{\partial x_3} H_2(x_1, x_3|\omega)\bigg|_{x_3=0} = 0 \tag{7.2}$$

on the surface of the perfect conductor. A solution of Eq. (7.1) that vanishes as $x_3 \to \infty$ is

$$H_2(x_1, x_3|\omega) = A \exp[ikx_1 - \beta_0(k)x_3], \tag{7.3}$$

where

$$\beta_0(k) = \begin{cases} [k^2 - (\omega/c)^2]^{\frac{1}{2}} & k^2 > (\omega/c)^2, \\ -i[(\omega/c)^2 - k^2]^{\frac{1}{2}} & k^2 < (\omega/c)^2. \end{cases} \tag{7.4}$$

For the expression (7.3) to represent a surface wave $\beta_0(k)$ should be real and positive, so that, from Eq. (7.4), we see that the wavenumber k should satisfy the inequality $|k| > (\omega/c)$.

Substitution of this solution into the boundary condition (7.2) yields the equation

$$-\beta_0(k) A \exp(ikx_1) = 0. \tag{7.5}$$

A nontrivial solution with $A \neq 0$ requires that $\beta_0(k) = 0$, which yields the dispersion relation

$$\omega = ck. \tag{7.6}$$

Modern Plasmonics. http://dx.doi.org/10.1016/B978-0-444-59526-3.00007-0

However, this dispersion relation does not correspond to a surface wave. When it is satisfied the magnetic field in the vacuum is given by

$$H_2(x_1, x_3|\omega) = A \exp[i(\omega/c)x_1], \tag{7.7}$$

independent of x_3. The wave described by Eq. (7.7) is in fact a surface skimming p-polarized bulk electromagnetic wave, not a surface electromagnetic wave.

However, if the perfectly conducting surface is roughened, either periodically or randomly, it supports a surface electromagnetic wave. This has been known for a long time in the context of the use of surface electromagnetic waves on metallic surfaces in technological applications in the gigahertz and terahertz regions of the electromagnetic spectrum.

In the gigahertz and terahertz spectral regions the electromagnetic field of a surface plasmon polariton at a planar vacuum-metal interface penetrates a distance of the order of 1 μm into the metal, but extends many hundreds or even thousands of wavelengths into the vacuum. Thus, this mode is very weakly bound to the interface, and is often referred to as a surface current. If it is desired to use surface electromagnetic waves in technological applications in these spectral regions, a way must be found to bind them to the surface.

A planar metal surface in these frequency regions, if structured with a periodic array of subwavelength grooves or dimples, can support a surface electromagnetic wave that is tightly bound to the dielectric-metal interface. The grooves and dimples allow some of the field in these modes to penetrate more deeply into the metal. This alters the electromagnetic boundary conditions away from those at a planar interface in a manner that allows a surface wave to exist. Surface electromagnetic waves in the visible region of the optical spectrum have been well studied and utilized. Structured metal surfaces now offer the possibility of studying and utilizing surface electromagnetic waves in the gigahertz and terahertz spectral regions as well. Since in the gigahertz and terahertz regions a metal is well described by a perfect conductor, the early calculations of surface waves on structured vacuum-metal interfaces in these frequency regions were carried out on the basis of a perfectly conducting surface.

Thus, Goubau [7.1] showed that although a perfectly conducting wire of circular cross section does not support a surface electronic wave, it does if it is periodically corrugated. Soon after, Rotman [7.2] showed theoretically and experimentally that a lamellar grating ruled on a metal surface will support a microwave surface electromagnetic wave.

In this early work it was also found that random surface roughness as well as periodic corrugations binds a surface electromagnetic wave to a perfectly conducting surface [7.3].

Many years later [7.4,7.5] it was noted that by using the results obtained by patterning a planar interface between a dielectric and a perfect conductor with one- or two-dimensional periodic arrays of grooves and holes of finite depth, respectively, one could create surface electromagnetic waves on metallic surfaces, in the microwave and terahertz frequency regions, that mimic the properties of surface plasmon polaritons at a planar dielectric-metal interface in the visible frequency range of the electromagnetic spectrum in a specified way by varying the parameters defining the patterning. This observation has opened the door to the creation of surface wave-based devices that operate at microwave and terahertz frequencies. Consequently these surface waves have become the objects of many theoretical and experimental investigations.

In this chapter we survey the theoretical and experimental studies that have been carried out of surface electromagnetic waves on periodically corrugated perfectly conducting surfaces. Applications of these surface waves are described in other chapters of this book.

We will restrict our discussion to surface electromagnetic waves on periodically structured surfaces that are planar in the absence of the structuring. This excludes consideration of surface waves on perfectly conducting milled [7.6,7.7] and helically grooved [7.8] wires, and on corrugated grooves [7.9] and ridges [7.10]. A comprehensive review of surface waves on these types of surfaces is presented in Ref. [7.11].

We also omit discussion of surface electromagnetic waves on randomly rough perfectly conducting surfaces. Theoretical results demonstrating the binding of such waves to one-dimensional and two-dimensional randomly rough perfectly conducting surfaces are presented in Refs. [7.12–7.14] and [7.15], respectively.

7.1 One-Dimensional Perfectly Conducting Surfaces: Theory

The dispersion curves and associated electromagnetic fields of surface electromagnetic waves on one-dimensional periodically corrugated perfectly conducting surfaces, defined by a variety of surface profile functions, have been calculated by several different approaches. Thus, dispersion curves have been calculated for surfaces defined by rectangular grooves [7.5,7.16–7.21], by a sinusoidal surface profile [7.22,7.23], by a symmetric sawtooth surface profile function [7.22], by a periodic array of V-grooves [7.24], by a periodic array of slits in a perfectly conducting film that is surrounded symmetrically [7.25,7.26] or asymmetrically [7.26]. Most of these calculations predicted dispersion curves with only one branch in the non-radiative region of the (ω, k) plane. However, in Refs. [7.18–7.21,7.23] it was found that for sufficiently deep grooves a perfectly conducting grating supports additional, higher frequency, branches of the dispersion curve. A dispersion curve with two branches has been predicted for surface electromagnetic waves on a doubly periodic groove array on a perfectly conducting surface [7.27].

Several of these calculations were carried out three to four decades ago for the mathematically identical problem of the propagation of surface acoustic waves of shear horizontal polarization on periodically corrugated surfaces of elastically isotropic media [7.16–7.18,7.22,7.23]. One needs only to replace the speed of shear elastic waves with the speed of light in vacuum to obtain the former curves from the latter.

In the remainder of this section we present an approach to the determination of the dispersion relation for surfaces on the one-dimensional periodically structured perfectly conducting surface depicted in Fig. 7.1. It is analogous to the method used by Lopez-Rios *et al.* [7.28] to study the reflectivity of a metallic lamellar grating but here applied to the corresponding homogeneous problem for a perfectly conducting lamellar grating.

We work with the single nonzero component of the magnetic field in this system, $H_2(x_1, x_3; t) = H_2(x_1, x_3|\omega) \exp(-i\omega t)$. Because this field must satisfy the Floquet-Bloch condition $H_2(x_1 + d, x_3|\omega) = \exp(ikd) H_2(x_1, x_3|\omega)$, where k is the wave number of the surface wave, the field at any point of space above the grating surface can be determined from the field in the central cell located between $x_1 = -d/2$ and $x_1 = d/2$.

In the vacuum region $x_3 > 0$, the magnetic field can be written in the form

$$H_2(x_1, x_3|\omega) = \sum_{n=-\infty}^{\infty} A_n \exp[ik_n x_1 + i\alpha_0(k_n) x_3], \tag{7.8}$$

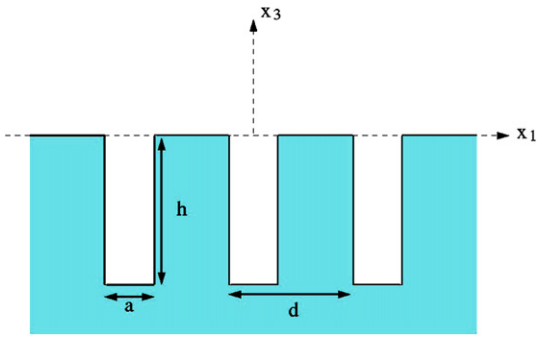

FIGURE 7.1

A perfectly conducting lamellar grating.

where $k_n = k + (2\pi n/d)$, and

$$\alpha_0(k_n) = [(\omega/c)^2 - k_n^2]^{\frac{1}{2}}, \quad Re\alpha_0(k_n) > 0, \quad Im\,\alpha_0(k_n) > 0. \tag{7.9}$$

We see from Eq. (7.8) that in order that the magnetic field it represents decay to zero as $x_3 \to \infty$, we must have $Im\alpha_0(k_n) > 0$.

The magnetic field within the central groove of the grating, which is defined by $-a/2 < x_1 < a/2$, $-h < x_3 < 0$, that satisfies the boundary conditions

$$\frac{\partial}{\partial x_1} H_2(\pm a/2, x_3|\omega) = 0 \qquad -h < x_3 < 0, \tag{7.10a}$$

$$\frac{\partial}{\partial x_3} H_2(x_1, -h|\omega) = 0 \qquad -a/2 < x_1 < a/2, \tag{7.10b}$$

can be written as

$$H_2(x_1, x_3|\omega) = \sum_{m=0}^{\infty} B_m \cos\frac{m\pi}{a}\left(x_1 - \frac{a}{2}\right)\cos\alpha_m(x_3 + h), \tag{7.11}$$

where

$$\alpha_m(\omega) = [(\omega/c)^2 - (m\pi/a)^2]^{\frac{1}{2}}, \; Re\alpha_m(\omega) > 0, \; Im\alpha_m(\omega) > 0. \tag{7.12}$$

The coefficients $\{A_n\}$ and $\{B_m\}$ are obtained from the remaining boundary conditions satisfied by the magnetic field. These are

$$\frac{\partial}{\partial x_3} H_2(x_1, 0+|\omega) = 0 \quad a/2 < |x_1| < d/2, \tag{7.13a}$$

$$H_2(x_1, 0+|\omega) = H_2(x_1, 0-|\omega) \quad -a/2 < x_1 < a/2, \tag{7.13b}$$

$$\frac{\partial}{\partial x_3} H_2(x_1, 0+|\omega) = \frac{\partial}{\partial x_3} H_2(x_1, 0-|\omega) \quad -a/2 < x_1 < a/2. \tag{7.13c}$$

We now project Eq. (7.13c) onto the set of basis vectors $\{\exp(-ik_j x_1);\ j = 0, \pm 1, \pm 2, \ldots\}$ with the use of Eq. (7.13a), and obtain

$$\int_{-\frac{d}{2}}^{\frac{d}{2}} dx_1 \frac{\partial}{\partial x_3} H_2(x_1, 0 + |\omega) \exp(-ik_j x_1)$$
$$= \int_{-\frac{a}{2}}^{\frac{a}{2}} dx_1 \frac{\partial}{\partial x_3} H_2(x_1, 0 - |\omega) \exp(-ik_j x_1), \tag{7.14}$$

where it should be kept in mind that the function represented by the integrand on the left-hand side of this equation vanishes for $|x_1| > a/2$. The substitution into this equation of the expressions given by Eqs. (7.8) and (7.11) then leads to

$$A_j = i\frac{a}{d}\frac{1}{\alpha_0(k_j)} \sum_{m=0}^{\infty} S_{jm}\alpha_m \sin\alpha_m h B_m, \tag{7.15}$$

where

$$S_{jm} = \frac{1}{a}\int_{-\frac{a}{2}}^{\frac{a}{2}} dx_1 \exp(-ik_j x_1) \cos\frac{m\pi}{a}\left(x_1 - \frac{a}{2}\right),$$
$$= \frac{1}{a}\frac{2k_j}{k_j^2 - (m\pi/a)^2} \sin k_j\frac{a}{2} \qquad m \text{ even}, \tag{7.16a}$$
$$= \frac{i}{a}\frac{2k_j}{k_j^2 - (m\pi/a)^2} \cos k_j\frac{a}{2} \qquad m \text{ odd}. \tag{7.16b}$$

We next project Eq. (7.13b) onto the set of basis vectors $\{\cos\frac{m\pi}{a}\left(x_1 - \frac{a}{2}\right);\ m = 0, 1, 2, \ldots\}$ and obtain

$$B_m = \frac{2\epsilon_m}{\cos\alpha_m h} \sum_{n=-\infty}^{\infty} S_{nm}^* A_n, \tag{7.17}$$

where $\{\epsilon_m\}$ are numbers defined by

$$\epsilon_m = \begin{cases} \frac{1}{2} & m = 0, \\ 1 & m \geq 1. \end{cases} \tag{7.18}$$

At this point we can either substitute Eq. (7.17) into Eq. (7.15) to obtain an infinite system of linear homogeneous equations for the amplitudes $\{A_n\}$,

$$A_n = i\frac{2a}{\alpha_0(k_n)d} \sum_{j=-\infty}^{\infty} \left\{ \sum_{m=0}^{\infty} \epsilon_m S_{nm} S_{jm}^* \alpha_m \tan\alpha_m h \right\} A_j, \tag{7.19}$$

or we can substitute Eq. (7.15) into Eq. (7.17) to obtain an infinite system of linear homogeneous equations for the amplitudes $\{B_m\}$,

$$B_m = i\frac{a}{d}\frac{2\epsilon_m}{\cos\alpha_m h} \sum_{j=0}^{\infty} \left\{ \sum_{n=-\infty}^{\infty} \frac{S_{nm}^* S_{nj}}{\alpha_0(k_n)} \alpha_j \sin\alpha_j h \right\} B_j. \tag{7.20}$$

The solvability condition for either of these systems of homogeneous equations is the dispersion relation for the surface electromagnetic waves propagating on the perfectly conducting surface depicted in Fig. 7.1.

In general these dispersion relations have to be solved numerically. However, an approximate analytic solution of the dispersion relation can be obtained in the following way. We first assume that only the fundamental eigenmode is retained in the expansion (7.11), i.e. the only nonzero term in this expansion is the $m = 0$ term. In this case Eq. (7.20) becomes

$$1 = i\frac{a}{d}\frac{\omega}{c}\tan(\omega h/c)\sum_{n=-\infty}^{\infty}\frac{\mathrm{sinc}^2(k_n a/2)}{\alpha_0(k_n)}. \tag{7.21}$$

This approximation is valid when the wavelength $2\pi/k$ of the surface wave is much larger than the lateral size a of the grooves, namely when $k \ll 2\pi/a$. We next assume that only the term with $n = 0$ in the expansion (7.8) is nonzero. This is equivalent to assuming that the structure depicted in Fig. 7.1 is a homogeneous metamaterial. With this assumption Eq. (7.21) simplifies to

$$k = \frac{\omega}{c}\left[1 + \left(\frac{a}{d}\right)^2 \mathrm{sinc}^4\frac{ka}{2}\tan^2\left(\frac{\omega h}{c}\right)\right]^{\frac{1}{2}}. \tag{7.22}$$

For a narrow groove, where $(a/d) \ll 1$, we can replace $\mathrm{sinc}(ka/2)$ by unity, and obtain finally

$$k = \frac{\omega}{c}\left[1 + \left(\frac{a}{d}\right)^2 \tan^2\left(\frac{\omega h}{c}\right)\right]^{\frac{1}{2}}. \tag{7.23}$$

From the result given by Eq. (7.23) we can deduce several features of the dispersion curve in its dependence on the parameters defining the surface, namely a, h, and d. We see first that for $a = 0$ or $h = 0$, which correspond to a planar surface, $k = (\omega/c)$, so that the corresponding wave is not bound to the surface. We also see that for nonzero a and h, k is larger than ω/c, i.e. it is in the non-radiative region of the (ω, k) plane, and hence the wave is bound to the surface. The dispersion curve bends away from the vacuum light line $\omega = ck$ into the non-radiative region more strongly as the width of the groove a increases for fixed values of its depth h and of the period of the grating d. The dispersion curve bends away from the vacuum light line $\omega = ck$ into the non-radiative region more strongly as the depth of the groove h increases for fixed values of the width of the groove a and of the period of the grating d (Fig. 7.2a). The dispersion curve also bends away from the vacuum light line more strongly as the width of the groove increases for fixed values of h and d (Fig. 7.2b). Thus, the wave displays the phenomenon of wave slowing, i.e. its phase and group velocities fall progressively below that of the speed of light in vacuum as the wave number k increases. The wave number k becomes infinite when $(\omega h/c) = \pi/2$. Therefore, the maximum frequency of the mode is given by $\omega_{max} = (\pi/2)(c/h)$, which decreases with increasing groove depth. Thus, the structured one-dimensional perfectly conducting surface that corresponds to the dispersion relation [7.23] is approximately equivalent to the planar surface of a free electron metal, characterized by a dielectric function $\epsilon(\omega) = 1 - \left(\omega_p^2/\omega^2\right)$ whose plasma frequency is $\omega_p = (\pi/\sqrt{2})(c/h)$.

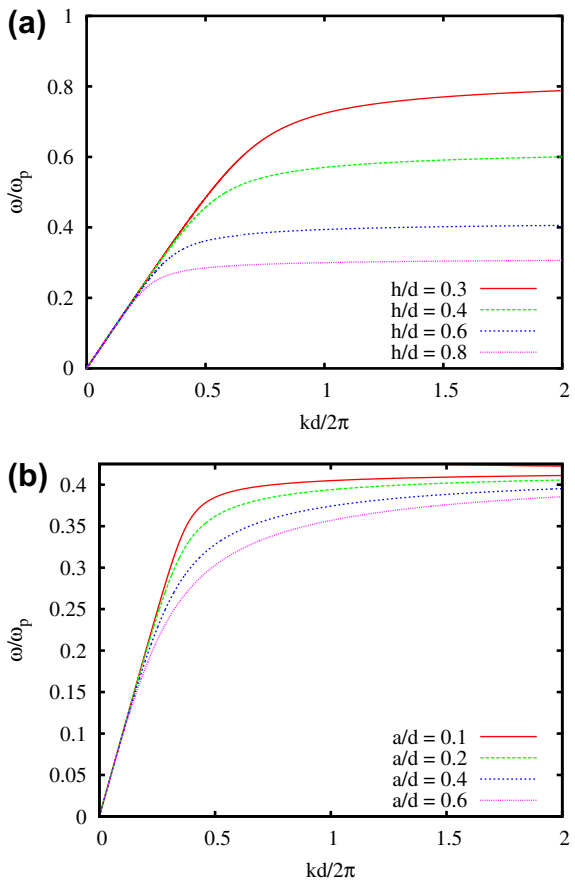

FIGURE 7.2

Dispersion curves for surface electromagnetic waves supported by the perfectly conducting lamellar grating depicted in Fig. 7.1. (a) Dependence on h for a fixed groove width $a = 0.2d$. (b) Dependence on a for a fixed groove depth $h/d = 0.6$.

7.2 Two-Dimensional Perfectly Conducting Surfaces: Theory

A good deal of attention has been directed at surface electromagnetic waves on two-dimensional periodically structured perfectly conducting surfaces. The majority of the theoretical studies of these waves have dealt with planar surfaces into which doubly periodic arrays of holes of finite [7.5,7.11,7.29–7.32] and infinite [7.4,7.5,7.33] depth have been drilled. In the majority of cases the holes have a square cross section, which simplifies the numerical calculations, e.g. by modal methods, and constitute a square array. However, holes with circular cross sections have been used in some calculations [7.29,7.33], and a

triangular lattice of circular holes was used in other calculations [7.29]. Other forms of two-dimensional periodically structured surfaces have also been used in such calculations [7.15,7.29,7.33–7.35].

In Refs. [7.4,7.5,7.33] the dispersion relation of the surface waves supported by two-dimensional periodically corrugated perfectly conducting surfaces was obtained from the pole of the reflectivity of the surface when the latter was illuminated from vacuum by a p-polarized electromagnetic field. In the remainder of this section we describe two approaches in which the dispersion relation is sought in a study of the free oscillations of the electromagnetic field in the vacuum region, rather than from the pole of the reflectivity. The first is a modal method analogous to the one used for this purpose in Refs. [7.11,7.32]. The second is the Rayleigh method [7.15] in which the electromagnetic field in the vacuum region is expanded in outgoing plane waves, and used in satisfying the boundary conditions on the structured surface. We consider them in turn.

7.2.1 A Modal Approach

The dispersion curve for surface electromagnetic waves with a square array of holes with a square cross section and a finite depth can be obtained by a modal method. The mathematical apparatus employed in this approach was developed in studies of the diffraction of electromagnetic waves by a thin perfectly conducting screen perforated by a two-dimensional periodic array of circular or rectangular holes, or the transmission of electromagnetic waves through such a periodically perforated perfectly conducting screen, by Chen [7.36–7.38] and by Bliek *et al.* [7.39].

The system we consider consists of a square lattice of lattice constant d of holes with a square cross section of edge a and a depth h drilled into the planar surface of a perfect conductor in contact with vacuum (Fig. 7.3). The vacuum occupies the region $x_3 > 0$, while the unstructured perfect conductor fills the region $x_3 < 0$. The surface profile function $\zeta(\mathbf{x}_\parallel)$ that defines the surface through the equation

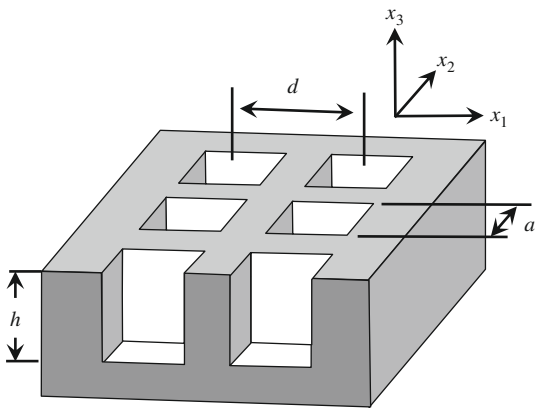

FIGURE 7.3

A schematic depiction of a two-dimensional square lattice of square holes of a finite depth drilled into a semi-infinite perfect conductor.

$x_3 = \zeta(\mathbf{x}_\parallel)$, where $\mathbf{x}_\parallel = (x_1, x_2, 0)$, is therefore a doubly periodic function of $\mathbf{x}_\parallel$,

$$\zeta(\mathbf{x}_\parallel + \mathbf{x}_\parallel(\ell)) = \zeta(\mathbf{x}_\parallel), \tag{7.24}$$

where

$$\mathbf{x}_\parallel(\ell) = \ell_1 \mathbf{a}_1 + \ell_2 \mathbf{a}_2. \tag{7.25}$$

Here $\mathbf{a}_1$ and $\mathbf{a}_2$ are two noncollinear primitive translation vectors of a two-dimensional Bravais lattice, while ℓ_1 and ℓ_2 are any positive or negative integers or zero, which we denote collectively by ℓ. The area of the primitive unit cell of the two-dimensional lattice defined by Eq. (7.25) is $a_c = |\mathbf{a}_1 \times \mathbf{a}_2|$.

The sites of the lattice reciprocal to the one defined by Eq. (7.25) is defined by

$$\mathbf{G}_\parallel(h) = h_1 \mathbf{b}_1 + h_2 \mathbf{b}_2, \tag{7.26}$$

where the primitive translation vectors $\mathbf{b}_1$ and $\mathbf{b}_2$ are defined by

$$\mathbf{a}_i \cdot \mathbf{b}_j = 2\pi \delta_{ij}, \tag{7.27}$$

where δ_{ij} is the Kronecker symbol, while h_1 and h_2 are any positive or negative integers and zero that we denote collectively by h. In the present case we have

$$\mathbf{a}_1 = d(1, 0, 0), \quad \mathbf{a}_2 = d(0, 1, 0), \tag{7.28a}$$

and

$$\mathbf{b}_1 = (2\pi/d)(1, 0, 0), \quad \mathbf{b}_2 = (2\pi/d)(0, 1, 0). \tag{7.28b}$$

The electric and magnetic fields in the region $x_3 > 0$ can be written as

$$\begin{aligned} \mathbf{E}^>(\mathbf{x}|\omega) = \sum_{\mathbf{G}_\parallel} \Bigg\{ & \left[\hat{\mathbf{K}}_\parallel - \hat{\mathbf{x}}_3 \frac{K_\parallel}{\alpha_0(K_\parallel, \omega)} \right] A_p(\mathbf{K}_\parallel) \\ & + (\hat{\mathbf{x}}_3 \times \hat{\mathbf{K}}_\parallel) A_s(\mathbf{K}_\parallel) \Bigg\} \phi(\mathbf{K}_\parallel|\mathbf{x}_\parallel) e^{i\alpha_0(K_\parallel,\omega)x_3}, \end{aligned} \tag{7.29a}$$

$$\begin{aligned} \mathbf{H}^>(\mathbf{x}|\omega) = \sum_{\mathbf{G}_\parallel} \Bigg\{ & \frac{\omega}{c} \frac{(\hat{\mathbf{x}}_3 \times \mathbf{K}_\parallel)}{\alpha_0(\mathbf{K}_\parallel, \omega)} A_p(\mathbf{K}_\parallel) \\ & - \frac{c}{\omega} \alpha_0(K_\parallel, \omega) \left[\hat{\mathbf{K}}_\parallel - \hat{\mathbf{x}}_3 \frac{K_\parallel}{\alpha_0(K_\parallel, \omega)} \right] A_s(\mathbf{K}_\parallel) \Bigg\} \\ & \times \phi(\mathbf{K}_\parallel|\mathbf{x}_\parallel) e^{i\alpha_0(K_\parallel,\omega)x_3}. \end{aligned} \tag{7.29b}$$

The superscript ">" in these expressions indicates that these are the fields in the vacuum region $x_3 > 0$. A time dependence of the form $\exp(-i\omega t)$ has been assumed in obtaining these fields, but is not indicated explicitly. To simplify the notation we have defined the wave vector $\mathbf{K}_\parallel$ by $\mathbf{K}_\parallel = \mathbf{k}_\parallel + \mathbf{G}_\parallel$, where $\mathbf{k}_\parallel = (k_1, k_2, 0)$ is the wave vector of the surface wave. The function $\alpha_0(\mathbf{K}_\parallel, \omega)$ is defined by

$$\alpha_0(\mathbf{K}_\parallel, \omega) = [(\omega/c)^2 - K_\parallel^2]^{\frac{1}{2}}, \ Re\alpha_0(K_\parallel, \omega) > 0, \ Im\alpha_0(K_\parallel, \omega) > 0. \tag{7.30}$$

The coefficients $\{A_p(\mathbf{K}_\parallel)\}$ and $\{A_s(\mathbf{K}_\parallel)\}$ are the amplitudes of the p(TM)—polarized and s(TE)-polarized components of the electromagnetic field in the region $x_3 > 0$, respectively. Finally, the functions $\{\phi(\mathbf{K}_\parallel|\mathbf{x}_\parallel)\}$ are the plane waves

$$\phi(\mathbf{K}_\parallel|\mathbf{x}_\parallel) = \frac{1}{d}\exp(i\mathbf{K}_\parallel \cdot \mathbf{x}_\parallel). \tag{7.31}$$

They are orthonormal when integrated over the area of the unit cell of the lattice of holes,

$$\int_0^d dx_1 \int_0^d dx_2 \phi^*(\mathbf{K}_\parallel|\mathbf{x}_\parallel)\phi(\mathbf{K}'_\parallel|\mathbf{x}_\parallel) = \delta_{\mathbf{K}_\parallel,\mathbf{K}'_\parallel}. \tag{7.32}$$

The tangential components of these electric and magnetic fields evaluated on the surface $x_3 = 0$, which are the components entering the boundary conditions at this surface, are then given by

$$E_1^>(\mathbf{x}_\parallel, 0|\omega) = \sum_{\mathbf{G}_\parallel}[\hat{K}_1 A_p(\mathbf{K}_\parallel) - \hat{K}_2 A_s(\mathbf{K}_\parallel)]\phi(\mathbf{K}_\parallel|\mathbf{x}_\parallel), \tag{7.33a}$$

$$E_2^>(\mathbf{x}_\parallel, 0|\omega) = \sum_{\mathbf{G}_\parallel}[\hat{K}_2 A_p(\mathbf{K}_\parallel) + \hat{K}_1 A_s(\mathbf{K}_\parallel)]\phi(\mathbf{K}_\parallel|\mathbf{x}_\parallel), \tag{7.33b}$$

$$H_1^>(\mathbf{x}_\parallel, 0|\omega) = \sum_{\mathbf{G}_\parallel}\left[-\frac{\omega}{c}\frac{\hat{K}_2}{\alpha_0(K_\parallel,\omega)}A_p(\mathbf{K}_\parallel) - \frac{c}{\omega}\alpha_0(K_\parallel,\omega)\hat{K}_1 A_s(\mathbf{K}_\parallel)\right]\phi(\mathbf{K}_\parallel|\mathbf{x}_\parallel), \tag{7.33c}$$

$$H_2^>(\mathbf{x}_\parallel, 0|\omega) = \sum_{\mathbf{G}_\parallel}\left[\frac{\omega}{c}\frac{\hat{K}_1}{\alpha_0(K_\parallel,\omega)}A_p(\mathbf{K}_\parallel) - \frac{c}{\omega}\alpha_0(K_\parallel,\omega)\hat{K}_2 A_s(\mathbf{K}_\parallel)\right]\phi(\mathbf{K}_\parallel|\mathbf{x}_\parallel). \tag{7.33d}$$

The electric and magnetic fields vanish inside the perfect conductor, but are nonzero inside the holes. The modes in the holes are waveguide modes when the holes are infinitely deep, and can be obtained by the approach described in the book by Jackson [7.40]. When the holes have a finite depth h, suitable linear combinations of these waveguide modes are used to satisfy the boundary conditions at $x_3 = -h$. In what follows we will assume that the holes have a finite depth h (Fig. 7.3).

The resulting modes can be divided into TE and TM modes, whose components can be written in the following forms ($m, n = 0, 1, 2, \ldots$):

TM modes

$$E_{1mn}^{\mathrm{TM}}(\mathbf{x}|\omega) = -\frac{k_{mn}}{\gamma_{mn}^2}\frac{m\pi}{a}\cos\frac{m\pi}{a}x_1 \sin\frac{n\pi}{a}x_2 \sin k_{mn}(x_3 + h), \tag{7.34a}$$

$$E_{2mn}^{\mathrm{TM}}(\mathbf{x}|\omega) = -\frac{k_{mn}}{\gamma_{mn}^2}\frac{n\pi}{a}\sin\frac{m\pi}{a}x_1 \cos\frac{n\pi}{a}x_2 \sin k_{mn}(x_3 + h), \tag{7.34b}$$

$$E_{3mn}^{\mathrm{TM}}(\mathbf{x}|\omega) = \sin\frac{m\pi}{a}x_1 \sin\frac{n\pi}{a}x_2 \cos k_{mn}(x_3 + h). \tag{7.34c}$$

$$H_{1mn}^{\mathrm{TM}}(\mathbf{x}|\omega) = -i\frac{(\omega/c)}{\gamma_{mn}^2}\frac{n\pi}{a}\sin\frac{m\pi}{a}x_1\cos\frac{n\pi}{a}x_2\cos k_{mn}(x_3+h), \tag{7.35a}$$

$$H_{2mn}^{\mathrm{TM}}(\mathbf{x}|\omega) = i\frac{(\omega/c)}{\gamma_{mn}^2}\frac{m\pi}{a}\cos\frac{m\pi}{a}x_1\sin\frac{n\pi}{a}x_2\cos k_{mn}(x_3+h), \tag{7.35b}$$

$$H_{3mn}^{\mathrm{TM}}(\mathbf{x}|\omega) = 0. \tag{7.35c}$$

TE modes

$$E_{1mn}^{\mathrm{TE}}(\mathbf{x}|\omega) = -i\frac{(\omega/c)}{\gamma_{mn}^2}\frac{n\pi}{a}\cos\frac{m\pi}{a}x_1\sin\frac{n\pi}{a}x_2\sin k_{mn}(x_3+h), \tag{7.36a}$$

$$E_{2mn}^{\mathrm{TE}}(\mathbf{x}|\omega) = i\frac{(\omega/c)}{\gamma_{mn}^2}\frac{m\pi}{a}\sin\frac{m\pi}{a}x_1\cos\frac{n\pi}{a}x_2\sin k_{mn}(x_3+h), \tag{7.36b}$$

$$E_{3mn}^{\mathrm{TE}}(\mathbf{x}|\omega) = 0. \tag{7.36c}$$

$$H_{1mn}^{\mathrm{TE}}(\mathbf{x}|\omega) = -\frac{k_{mn}}{\gamma_{mn}^2}\frac{m\pi}{a}\sin\frac{m\pi}{a}x_1\cos\frac{n\pi}{a}x_2\cos k_{mn}(x_3+h), \tag{7.37a}$$

$$H_{2mn}^{\mathrm{TE}}(\mathbf{x}|\omega) = -\frac{k_{mn}}{\gamma_{mn}^2}\frac{n\pi}{a}\cos\frac{m\pi}{a}x_1\sin\frac{n\pi}{a}x_2\cos k_{mn}(x_3+h), \tag{7.37b}$$

$$H_{3mn}^{\mathrm{TE}}(\mathbf{x}|\omega) = \cos\frac{m\pi}{a}x_1\cos\frac{n\pi}{a}x_2 sin k_{mn}(x_3+h). \tag{7.37c}$$

In these expressions we have introduced the functions

$$\gamma_{mn} = \left[\left(\frac{m\pi}{a}\right)^2 + \left(\frac{n\pi}{a}\right)^2\right]^{\frac{1}{2}}, \tag{7.38}$$

$$k_{mn} = \left[(\omega/c)^2 - \gamma_{mn}^2\right]^{\frac{1}{2}}. \tag{7.39}$$

The tangential components of the electric and magnetic fields in the region $x_3 < 0$ evaluated on the plane $x_3 = 0$ can then be written as

$$E_1^<(\mathbf{x}_\parallel, 0|\omega) = \sum_{m=0}^{\infty}\sum_{n=0}^{\infty}\left[A_{mn}\left(-\frac{k_{mn}}{\gamma_{mn}^2}\frac{m\pi}{a}\right) + B_{mn}\left(-i\frac{(\omega/c)}{\gamma_{mn}^2}\frac{n\pi}{a}\right)\right]\cos\frac{m\pi}{a}x_1\sin\frac{n\pi}{a}x_2\sin k_{mn}h, \tag{7.40a}$$

$$E_2^<(\mathbf{x}_\parallel, 0|\omega) = \sum_{m=0}^{\infty}\sum_{n=0}^{\infty}\left[A_{mn}\left(-\frac{k_{mn}}{\gamma_{mn}^2}\frac{n\pi}{a}\right) + B_{mn}\left(i\frac{(\omega/c)}{\gamma_{mn}^2}\frac{m\pi}{a}\right)\right]\sin\frac{m\pi}{a}x_1\cos\frac{n\pi}{a}x_2\sin k_{mn}h, \tag{7.40b}$$

$$H_1^<(\mathbf{x}_\parallel, 0|\omega) = \sum_{m=0}^{\infty}\sum_{n=0}^{\infty}\left[A_{mn}\left(-i\frac{(\omega/c)}{\gamma_{mn}^2}\frac{n\pi}{a}\right)\right.$$
$$\left.+B_{mn}\left(-\frac{k_{mn}}{\gamma_{mn}^2}\frac{m\pi}{a}\right)\right]\sin\frac{m\pi}{a}x_1\cos\frac{n\pi}{a}x_2\cos k_{mn}h, \tag{7.40c}$$

$$H_2^<(\mathbf{x}_\parallel, 0|\omega) = \sum_{m=0}^{\infty}\sum_{n=0}^{\infty}\left[A_{mn}\left(i\frac{(\omega/c)}{\gamma_{mn}^2}\frac{m\pi}{a}\right)\right.$$
$$\left.+B_{mn}\left(-\frac{k_{mn}}{\gamma_{mn}^2}\frac{n\pi}{a}\right)\right]\cos\frac{m\pi}{a}x_1\sin\frac{n\pi}{a}x_2\cos k_{mn}h, \tag{7.40d}$$

where the $\{A_{mn}\}$ and $\{B_{mn}\}$ are coefficients to be determined. It should be kept in mind that these field components are nonzero only in the region $0 < x_1 < a, 0 < x_2 < a$.

The boundary conditions on the fields at the plane $x_3 = 0$ require that $E_1^>(\mathbf{x}_\parallel, 0|\omega)$ and $E_2^>(\mathbf{x}_\parallel, 0|\omega)$ vanish on this plane outside the region of the unit cell occupied by the hole, and be continuous across the hole:

$$E_\alpha^>(\mathbf{x}_\parallel, 0|\omega) = E_\alpha^<(\mathbf{x}_\parallel, 0|\omega) \quad \alpha = 1, 2. \tag{7.41}$$

They also require that H_1 and H_2 be continuous across the hole:

$$H_\alpha^>(\mathbf{x}_\parallel, 0|\omega) = H_\alpha^<(\mathbf{x}_\parallel, 0|\omega) \quad \alpha = 1, 2. \tag{7.42}$$

We use these equations to obtain relations among the amplitudes $A_p(\mathbf{K}_\parallel)$, $A_s(\mathbf{K}_\parallel)$, A_{mn}, and B_{mn}. We first project Eq. (7.41) on the function $\phi^*(\mathbf{K}'_\parallel|\mathbf{x}_\parallel)$ and obtain

$$[\hat{K}_1 A_p(\mathbf{K}_\parallel) - \hat{K}_2 A_s(\mathbf{K}_\parallel)]$$
$$= \sum_{m=0}^{\infty}\sum_{n=0}^{\infty}\left[A_{mn}\left(-\frac{k_{mn}}{\gamma_{mn}^2}\frac{m\pi}{a}\right) + B_{mn}\left(-i\frac{(\omega/c)}{\gamma_{mn}^2}\frac{n\pi}{a}\right)\right]$$
$$\times \sin k_{mn}h S_{mn}^*(\mathbf{K}_\parallel), \tag{7.43a}$$

$$[\hat{K}_2 A_p(\mathbf{K}_\parallel) + \hat{K}_2 A_s(\mathbf{K}_\parallel)]$$
$$= \sum_{m=0}^{\infty}\sum_{n=0}^{\infty}\left[A_{mn}\left(-\frac{k_{mn}}{\gamma_{mn}^2}\frac{n\pi}{a}\right) + B_{mn}\left(-i\frac{(\omega/c)}{\gamma_{mn}^2}\frac{m\pi}{a}\right)\right]$$
$$\times \sin k_{mn}h T_{mn}^*(\mathbf{K}_\parallel), \tag{7.43b}$$

where

$$S_{mn}(\mathbf{K}_\parallel) = \int_0^a dx_1 \int_0^a dx_2 \phi(\mathbf{K}_\parallel|\mathbf{x}_\parallel)\cos\frac{m\pi}{a}x_1\sin\frac{n\pi}{a}x_2, \tag{7.44a}$$

$$T_{mn}(\mathbf{K}_\parallel) = \int_0^a dx_1 \int_0^a dx_2 \phi(\mathbf{K}_\parallel|\mathbf{x}_\parallel)\sin\frac{m\pi}{a}x_1\cos\frac{n\pi}{a}x_2. \tag{7.44b}$$

These integrals can be evaluated analytically in closed form.

We then project Eq. (7.42) with $\alpha = 1$ on the function $\sin \frac{m'\pi}{a} x_1 \cos \frac{n'\pi}{a} x_2$, and obtain

$$\sum_{\mathbf{G}_\parallel} \left[-\frac{\omega}{c} \frac{\hat{K}_2}{\alpha_0(K_\parallel, \omega)} A_p(\mathbf{K}_\parallel) - \frac{c}{\omega} \alpha_0(K_\parallel, \omega) \hat{K}_1 A_s(\mathbf{K}_\parallel) \right] T_{mn}(\mathbf{K}_\parallel)$$
$$= \frac{a^2}{4} \theta_m \epsilon_n \left[A_{mn} \left(-i \frac{(\omega/c)}{\gamma_{mn}^2} \frac{n\pi}{a} \right) + B_{mn} \left(-\frac{k_{mn}}{\gamma_{mn}^2} \frac{m\pi}{a} \right) \right]. \tag{7.45a}$$

We next project Eq. (7.42) with $\alpha = 2$ on the function $\cos \frac{m'\pi}{a} x_1 \sin \frac{n'\pi}{a} x_2$ and obtain

$$\sum_{\mathbf{G}_\parallel} \left[\frac{\omega}{c} \frac{\hat{K}_1}{\alpha_0(K_\parallel, \omega)} A_p(\mathbf{K}_\parallel) - \frac{c}{\omega} \alpha_0(K_\parallel, \omega) \hat{K}_2 A_s(\mathbf{K}_\parallel) \right] S_{mn}(\mathbf{K}_\parallel)$$
$$= \frac{a^2}{4} \epsilon_m \theta_n \left[A_{mn} \left(i \frac{(\omega/c)}{\gamma_{mn}^2} \frac{m\pi}{a} \right) + B_{mn} \left(-\frac{k_{mn}}{\gamma_{mn}^2} \frac{n\pi}{a} \right) \right]. \tag{7.45b}$$

In writing these equations we have introduced the symbols

$$\theta_m = (1 - \delta_{m0}) \qquad m \geq 0 \tag{7.46}$$

and

$$\epsilon_0 = 2 \tag{7.47a}$$
$$\epsilon_m = 1 \qquad m \geqslant 1. \tag{7.47b}$$

The pair of Eqs. (7.45) can be solved to yield A_{mn} and B_{mn} as functions of $A_p(\mathbf{K}_\parallel)$ and $A_s(\mathbf{K}_\parallel)$. When these relations are substituted into Eqs. (7.43) a pair of coupled homogeneous equations for $A_p(\mathbf{K}_\parallel)$ and $A_s(\mathbf{K}_\parallel)$ is obtained. The solvability condition for this system of equations is the dispersion relation for the surface waves supported by the doubly periodically corrugated perfectly conducting surface.

In order that the dispersion relation obtained in this way be the dispersion relation for a surface electromagnetic wave, its solution should be sought in the non-radiative region of the $(\omega, \mathbf{k}_\parallel)$ plane, which is defined by the condition $k_\parallel > \omega/c$. In this region $\alpha_0(\mathbf{K}_\parallel)$ is pure imaginary for each value of $\mathbf{K}_\parallel$, and the electromagnetic fields defined by Eqs. (7.29) decay exponentially with increasing distance into the vacuum from the surface $x_3 = 0$.

As an illustration of the kinds of results that can be obtained by this approach we present in Fig. 7.4a dispersion curves of the surface electromagnetic waves supported by a square lattice of lattice constant d of square holes of edge a of different depths h [7.11]. These curves are plotted for a value of a given by $a = 0.6d$, and for values of h increasing from $h = 0.1d$ to $h = d$. The two-dimensional wave vector of the surface wave is assumed to be given by $\mathbf{k}_\parallel = \hat{\mathbf{x}}_1 k_\parallel$. The dispersion curve is a periodic function of $k_\parallel$ with a period $2\pi/d$. It is an even function of $k_\parallel$, is tangent to the vacuum light line $\omega = ck_\parallel$ as $k_\parallel \to 0$, and has a zero slope at $k_\parallel = \pi/d$. It thus mimics the dispersion curve of a surface plasmon polariton propagating on a planar metallic surface.

It is seen that the dispersion curve is lowered in frequency as the depth of the hole is increased. It is also lowered in frequency when the ratio a/d is increased from $a/d = 0.4$ to $a/d = 0.8$, when the depth h is kept fixed at $h = 0.6d$ (Fig. 7.4b).

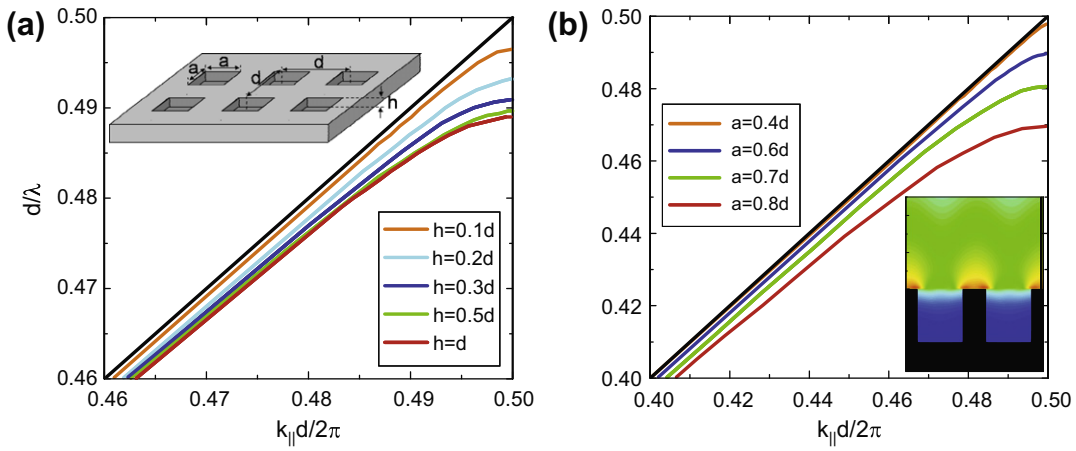

FIGURE 7.4

The dispersion curve of the surface electromagnetic waves supported by a square lattice of square holes of finite depth drilled into the planar surface of a perfect conductor. The length of the edge of a hole is related to the lattice constant of the square lattice by $a = 0.6d$. The depth of the holes increases from $h = 0.1d$ to $h = d$. The inset shows a schematic of the system. (b) Dispersion curves for this system when the hole depth is fixed at $h = 0.6d$ and the length of the edge increases from $a = 0.4d$ to $a = 0.8d$. The inset shows the electric field amplitude at the band edge for $h = 0.6d$ and $a = 0.6d$ (Ref. [7.11]).

Thus, by varying the geometrical properties of a doubly periodic array of holes of finite depth drilled into the planar surface of a semi-infinite perfect conductor, surface electromagnetic waves can be produced on it with tailored dispersion curves that resemble those of surface plasmon polaritons on a planar metal surface.

7.2.2 The Rayleigh Method

The modal method is particularly well-suited to the determination of the dispersion relation of surface electromagnetic waves on a perfectly conducting surface pierced by a doubly periodic array of holes of finite depth.

However, these are not the only kinds of periodically structured perfectly conducting surfaces that support surface electromagnetic waves. Such surfaces with more general profile functions can also support surface waves, whose dispersion relations can be obtained by an approach that differs from the modal method, namely the Rayleigh method [7.41]. In this method the expression for the electromagnetic field in the vacuum region that satisfies the boundary condition at infinity, is continued into the surface, and used to satisfy the boundary conditions on it. In the selvedge region, the region of the vacuum between the minimum and maximum points on the surface, the electromagnetic field can consist of both incoming and outgoing waves, while in the Rayleigh method it consists of only outgoing waves. Nevertheless, it has been shown by many authors [7.42–7.49] that it is a rigorous approach to the study of the interaction of an electromagnetic field with a periodically structured surface provided that the

surface profile function is an analytic function of its coordinates, and that the ratio of the amplitude of the surface structure to the period of the structure is smaller than a critical value. Methods for determining this critical ratio have been developed [7.44,7.46,7.49].

In this section we will apply the Rayleigh method to obtain the dispersion relation for the free oscillations of the electromagnetic field in the vacuum above the rough surface. As we have noted earlier, this is equivalent to investigating the poles of the specular reflectivity, and leads to somewhat simpler calculations. We first use this approach to determine the dispersion relation for a rough perfectly conducting surface defined by an arbitrary two-dimensional profile function. We then specialize the result to the case that the rough surface is a bigrating.

7.2.2.1 The Rayleigh Dispersion Relation

When the perfectly conducting surface is a two-dimensional rough surface, we write the equation defining the surface as $x_3 = \zeta(\mathbf{x}_\parallel)$. The region $x_3 > \zeta(\mathbf{x}_\parallel)$ is vacuum. The region $x_3 < \zeta(\mathbf{x}_\parallel)$ is the perfect conductor. The surface profile function $\zeta(\mathbf{x}_\parallel)$ is assumed to be a single-valued function of $\mathbf{x}_\parallel$ that is differentiable with respect to x_1 and x_2.

The electric field in the vacuum region can be written as $\mathbf{E}(\mathbf{x};t) = \mathbf{E}(\mathbf{x}|\omega)\exp(-i\omega t)$, where

$$\mathbf{E}(\mathbf{x}|\omega) = \int \frac{d^2q_\parallel}{(2\pi)^2}\left\{\frac{c}{\omega}[\hat{\mathbf{q}}_\parallel\alpha_0(q_\parallel) - \hat{\mathbf{x}}_3 q_\parallel]A_p(\mathbf{q}_\parallel) + (\hat{\mathbf{x}}_3\times\hat{\mathbf{q}}_\parallel)A_s(\mathbf{q}_\parallel)\right\}\exp[i\mathbf{q}_\parallel\cdot\mathbf{x}_\parallel + i\alpha_0(q_\parallel)x_3], \tag{7.48}$$

with

$$\alpha_0(q_\parallel) = [(\omega/c)^2 - q_\parallel^2]^{\frac{1}{2}},\ \ Re\alpha_0(q_\parallel) > 0,\ \ Im\alpha_0(q_\parallel) > 0. \tag{7.49}$$

The coefficients $A_p(\mathbf{q}_\parallel)$ and $A_s(\mathbf{q}_\parallel)$ are the amplitudes of the p- and s-polarized components of this field with respect to the local sagittal plane defined by the vectors $\hat{\mathbf{q}}_\parallel$ and $\hat{\mathbf{x}}_3$.

To obtain the dispersion relation for surface electromagnetic waves on this surface we begin by introducing the vector

$$\mathbf{J}_E(\mathbf{x}_\parallel|\omega) = \mathbf{n}\times\mathbf{E}(\mathbf{x}|\omega)\,|_{x_3=\zeta(\mathbf{x}_\parallel)}\,, \tag{7.50}$$

where

$$\mathbf{n} = (-\zeta_1(\mathbf{x}_\parallel), -\zeta_2(\mathbf{x}_\parallel), 1) \tag{7.51}$$

is a vector normal to the surface at each point of it, directed into the vacuum, and $\zeta_j(\mathbf{x}_\parallel) = \partial\zeta(\mathbf{x}_\parallel)/\partial x_j$, $j = 1, 2$.

The boundary condition satisfied by the field (7.44) on the surface $x_3 = \zeta(\mathbf{x}_\parallel)$ can now be written

$$\mathbf{J}_E(\mathbf{x}_\parallel|\omega) = 0. \tag{7.52}$$

This vector equation constitutes a set of three equations

$$J_E(\mathbf{x}_\parallel|\omega)_i = 0 \quad i = 1, 2, 3. \tag{7.53}$$

However, these equations are not independent. The vector $\mathbf{n}$ is perpendicular to the vector $\mathbf{J}_E(\mathbf{x}_\parallel|\omega)$, so that

$$\mathbf{n}\cdot\mathbf{J}_E(\mathbf{x}_\parallel|\omega) = -\zeta_1(\mathbf{x}_\parallel)J_E(\mathbf{x}_\parallel|\omega)_1 - \zeta_2(\mathbf{x}_\parallel J_E(\mathbf{x}_\parallel|\omega)_2 + J_E(\mathbf{x}_\parallel|\omega)_3 = 0. \tag{7.54}$$

Thus, the satisfaction of any two of Eqs. (7.53) ensures the satisfaction of the third. We will assume as the pair of independent equations Eq. (7.53) with $i = 1, 2$. Written out explicitly, they are

$$\int \frac{d^2q_\parallel}{(2\pi)^2}\left\{\frac{c}{\omega}[q_\parallel\zeta_2(\mathbf{x}_\parallel) - \hat{q}_2\alpha_0(q_\parallel)]A_p(\mathbf{q}_\parallel) - \hat{q}_1 A_s(\mathbf{q}_\parallel)\right\}\exp[i\mathbf{q}_\parallel\cdot\mathbf{x}_\parallel + i\alpha_0(q_\parallel)\zeta(\mathbf{x}_\parallel)] = 0, \tag{7.55a}$$

$$\int \frac{d^2q_\parallel}{(2\pi)^2}\left\{\frac{c}{\omega}[\hat{q}_1\alpha_0(q_\parallel) - q_\parallel\zeta_1(\mathbf{x}_\parallel)]A_p(\mathbf{q}_\parallel) - \hat{q}_2 A_s(\mathbf{q}_\parallel)\right\}\exp[i\mathbf{q}_\parallel\cdot\mathbf{x}_\parallel + i\alpha_0(q_\parallel)\zeta(\mathbf{x}_\parallel)] = 0. \tag{7.55b}$$

We next introduce the representation

$$\exp[i\gamma\zeta(\mathbf{x}_\parallel)] = \int \frac{d^2Q_\parallel}{(2\pi)^2} I(\gamma|\mathbf{Q}_\parallel)\exp(i\mathbf{Q}_\parallel\cdot\mathbf{x}_\parallel), \tag{7.56}$$

so that

$$I(\gamma|\mathbf{Q}_\parallel) = \int d^2x_\parallel \exp(-i\mathbf{Q}_\parallel\cdot\mathbf{x}_\parallel)\exp[i\gamma\zeta(\mathbf{x}_\parallel)]. \tag{7.57}$$

By differentiating both sides of Eq. (7.57) with respect to $x_\mu(\mu = 1, 2)$, we obtain

$$\zeta_\mu(\mathbf{x}_\parallel)\exp[i\gamma\zeta(\mathbf{x}_\parallel)] = \int \frac{d^2Q_\parallel}{(2\pi)^2}\frac{Q_\mu}{\gamma} I(\gamma|\mathbf{Q}_\parallel)\exp(i\mathbf{Q}_\parallel\cdot\mathbf{x}_\parallel). \tag{7.58}$$

When we substitute Eqs. (7.56) and (7.58) into Eqs. (7.55a) and (7.55b), and equate to zero the $\mathbf{k}_\parallel$ Fourier coefficient in each of the resulting equations, we obtain the equations satisfied by the amplitudes $A_p(\mathbf{q}_\parallel)$ and $A_s(\mathbf{q}_\parallel)$,

$$\int \frac{d^2q_\parallel}{(2\pi)^2} I(\alpha_0(q_\parallel)|\mathbf{k}_\parallel - \mathbf{q}_\parallel) \times\left\{\frac{c}{\omega}\frac{q_\parallel k_\parallel\hat{k}_2 - (\omega/c)^2\hat{q}_2}{\alpha_0(q_\parallel)}A_p(\mathbf{q}_\parallel) - \hat{q}_1 A_s(\mathbf{q}_\parallel)\right\} = 0, \tag{7.59a}$$

$$\int \frac{d^2q_\parallel}{(2\pi)^2} I(\alpha_0(q_\parallel)|\mathbf{k}_\parallel - \mathbf{q}_\parallel) \times\left\{-\frac{c}{\omega}\frac{q_\parallel k_\parallel\hat{k}_1 - (\omega/c)^2\hat{q}_1}{\alpha_0(q_\parallel)}A_p(\mathbf{q}_\parallel) - \hat{q}_2 A_s(\mathbf{q}_\parallel)\right\} = 0. \tag{7.59b}$$

A more convenient set of equations for these amplitudes is obtained in the following way. We multiply Eq. (7.59a) by $\hat{k}_2$, Eq. (7.59b) by $-\hat{k}_1$, and add the resulting equations. The result is

$$\int \frac{d^2q_\parallel}{(2\pi)^2} I(\alpha_0(q_\parallel)|\mathbf{k}_\parallel - \mathbf{q}_\parallel) \left\{ \frac{c}{\omega} \frac{k_\parallel q_\parallel - (\omega/c)^2(\hat{\mathbf{k}}_\parallel \cdot \hat{\mathbf{q}}_\parallel)}{\alpha_0(q_\parallel)} A_p(\mathbf{q}_\parallel) + (\hat{\mathbf{k}}_\parallel \times \hat{\mathbf{q}}_\parallel)_3 A_s(\mathbf{q}_\parallel) \right\} = 0. \quad (7.60)$$

We next multiply Eq. (7.59a) by $\hat{k}_1$, Eq. (7.59b) by $\hat{k}_2$, and add the resulting equations. The result is

$$\int \frac{d^2q_\parallel}{(2\pi)^2} I(\alpha_0(q_\parallel)|\mathbf{k}_\parallel - \mathbf{q}_\parallel) \left\{ \frac{\omega}{c} \frac{(\hat{\mathbf{k}}_\parallel \times \hat{\mathbf{q}}_\parallel)_3}{\alpha_0(q_\parallel)} A_p(\mathbf{q}_\parallel) + (\hat{\mathbf{k}}_\parallel \cdot \hat{\mathbf{q}}_\parallel) A_s(\mathbf{q}_\parallel) \right\} = 0. \quad (7.61)$$

The solvability condition for this pair of coupled homogeneous integral equations for $A_p(\mathbf{q}_\parallel)$ and $A_s(\mathbf{q}_\parallel)$ is the dispersion relation for the surface electromagnetic waves on the surface $x_3 = \zeta(\mathbf{x}_\parallel)$. From Eq. (7.60) we see that for any solution $\omega(\mathbf{k}_\parallel)$ of this dispersion relation to be the dispersion curve of a surface wave, $Im\alpha_0(k_\parallel)$ must be positive.

7.2.2.2 A Doubly Periodic Surface

We now apply Eqs. (7.60) and (7.61) to the case where the surface profile function is a doubly periodic function of $\mathbf{x}_\parallel$, Eq. (7.24). For such a surface the function $I(\gamma|\mathbf{Q}_\parallel)$ becomes

$$I(\gamma|\mathbf{Q}_\parallel) = \sum_{\mathbf{G}_\parallel} (2\pi)^2 \delta(\mathbf{Q}_\parallel - \mathbf{G}_\parallel) \mathcal{I}(\gamma|\mathbf{G}_\parallel), \quad (7.62)$$

where

$$\mathcal{I}(\gamma|\mathbf{G}_\parallel) = \frac{1}{a_c} \int_{a_c} d^2x_\parallel \exp(-i\mathbf{G}_\parallel \cdot \mathbf{x}_\parallel) \exp[i\gamma\zeta(\mathbf{x}_\parallel)]. \quad (7.63)$$

We also introduce the expansions

$$A_{p,s}(\mathbf{q}_\parallel) = \sum_{\mathbf{G}_\parallel} (2\pi)^2 \delta(\mathbf{q}_\parallel - \mathbf{k}_\parallel - \mathbf{G}_\parallel) a_{p,s}(\mathbf{k}_\parallel + \mathbf{G}_\parallel), \quad (7.64)$$

where $\mathbf{k}_\parallel$ is the two-dimensional wave vector of the surface electromagnetic wave, in order that the electric field in the vacuum region satisfy the Bloch-Floquet theorem.

The substitution of the expansions (7.62) and (7.64) into Eqs. (7.60) and (7.61) yields the following equation for the coefficients $a_{p,s}(\mathbf{k}_\parallel + \mathbf{G}_\parallel)$:

$$\sum_{\mathbf{G}'_\parallel} \mathcal{I}(\alpha_0(\mathbf{K}'_\parallel)|\mathbf{K}_\parallel - \mathbf{K}'_\parallel) \times \begin{pmatrix} \frac{c}{\omega} \frac{K_\parallel K'_\parallel - (\omega/c)^2 \hat{\mathbf{K}}_\parallel \cdot \hat{\mathbf{K}}'_\parallel}{\alpha_0(K'_\parallel)} & (\hat{\mathbf{K}}_\parallel \times \hat{\mathbf{K}}'_\parallel)_3 \\ \frac{\omega}{c} \frac{(\hat{\mathbf{K}}_\parallel \times \hat{\mathbf{K}}'_\parallel)_3}{\alpha_0(K'_\parallel)} & (\hat{\mathbf{K}}_\parallel \cdot \hat{\mathbf{K}}'_\parallel) \end{pmatrix} \begin{pmatrix} a_p(\mathbf{K}'_\parallel) \\ a_s(\mathbf{K}'_\parallel) \end{pmatrix} = 0. \quad (7.65)$$

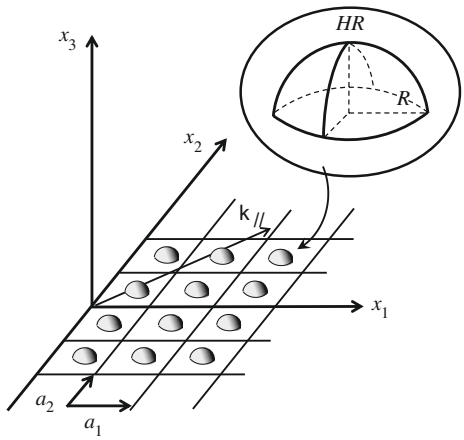

FIGURE 7.5

A doubly periodic surface formed by placing a square lattice of perfectly conducting hemiellipsoids on the planar surface of a semi-infinite perfect conductor.

In writing this equation we have introduced the vectors $\mathbf{K}_\parallel = \mathbf{k}_\parallel + \mathbf{G}_\parallel$ and $\mathbf{K}'_\parallel = \mathbf{k}_\parallel + \mathbf{G}'_\parallel$. The dispersion relation for surface electromagnetic waves on a perfectly conducting bigrating is obtained by equating to zero the determinant of the matrix of coefficients in Eq. (7.65).

The solutions of this dispersion relation are even functions of $\mathbf{k}_\parallel$, $\omega_s(-\mathbf{k}_\parallel) = \omega_s(\mathbf{k}_\parallel)$, where s labels the solutions (bands) for a given $\mathbf{k}_\parallel$ in the order of increasing magnitude. They are also periodic functions of $\mathbf{k}_\parallel$ with a period that is the first Brillouin zone of the bigrating, $\omega_s(\mathbf{k}_\parallel + \mathbf{G}_\parallel) = \omega_s(\mathbf{k}_\parallel)$. The solutions can then be sought for values of $\mathbf{k}_\parallel$ inside the first Brillouin zone, and inside the non-radiative region defined by $k_\parallel > (\omega/c)$.

Dispersion curves have been calculated for surface electromagnetic waves propagating on a surface that consists of a square lattice of hemiellipsoids on an otherwise planar surface of a perfect conductor (Fig. 7.5). The primitive translation vectors of the square lattice are $\mathbf{a}_1 = a(1, 0, 0)$, $\mathbf{a}_2 = a(0, 1, 0)$. Those of the reciprocal lattice are $\mathbf{b}_1 = (2\pi/a)(1, 0, 0)$, $\mathbf{b}_2 = (2\pi/a)(0, 1, 0)$. The surface profile function is given by

$$\zeta(\mathbf{x}_\parallel) = \sum_\ell s(\mathbf{x}_\parallel - \mathbf{x}_\parallel(\ell)), \tag{7.66}$$

where

$$s(\mathbf{x}_\parallel) = H[R^2 - x_\parallel^2]^{\frac{1}{2}} \qquad |\mathbf{x}_\parallel| < R, \tag{7.67a}$$

$$= 0 \qquad |\mathbf{x}_\parallel| > R. \tag{7.67b}$$

The function $\mathcal{I}(\gamma|\mathbf{G}_\parallel)$ defined by Eq. (7.63) in this case becomes

$$\mathcal{I}(\gamma|\mathbf{G}_\parallel) = 1 + \frac{2\pi R^2}{a^2} \sum_{n=1}^{\infty} \frac{(i\gamma H R)^n}{(n+2)n!} \quad \mathbf{G}_\parallel = 0, \tag{7.68a}$$

$$= \frac{2\pi R^2}{a^2} \sum_{n=1}^{\infty} \frac{(i\gamma HR)^n}{n!} \frac{2^{\frac{n}{2}}\Gamma\left(\frac{n}{2}+1\right)}{(G_{\|}R)^{\frac{n}{2}+1}} J_{\frac{n}{2}+1}(G_{\|}R)\mathbf{G}_{\|} \neq 0, \tag{7.68b}$$

where $J_\nu(x)$ is the Bessel function of the first kind and order ν.

Due to the circular symmetry of each hemiellipsoid, it is necessary to solve the dispersion relations only for vectors $\mathbf{k}_{\|}$ inside the irreducible element of the two-dimensional first Brillouin zone. In the present case it consists of the one-eighth region of the first Brillouin zone that generates the entire zone when transformed by the application of the operations of the point group C_{4v} to it. It is depicted in the insets to Fig. 7.6a and b.

In solving the dispersion relation defined by Eq. (7.65) the infinite sum over $\mathbf{G}'_{\|}$ has to be truncated. This was done by restricting the reciprocal lattice vectors $\mathbf{G}_{\|}(h) = h_1\mathbf{b}_1 + h_2\mathbf{b}_2$ and $\mathbf{G}'_{\|}(h') = h'_1\mathbf{b}_1 + h'_2\mathbf{b}_2$ to those that satisfied the conditions $\left[h_1^2 + h_2^2\right]^{\frac{1}{2}} \leq N_{max}$ and $\left[h_1'^2 + h_2'^2\right]^{\frac{1}{2}} \leq N_{max}$ for some integer N_{max}. The convergence of a solution was tested by increasing N_{max} systematically until the solution stopped changing.

The values of the parameters assumed in obtaining the results presented in Fig. 7.6a were $R/a = 0.375$ and $H = 1$, and for the results presented in Fig. 7.6b they were $R/a = 0.375$ and $H = -1$. The first 15 terms in the series in (7.68a) and (7.68b) were kept, and a value of $N_{max} = 10$ was used in calculating the results plotted in this figure. The dispersion curves depicted in this figure were calculated for values of $\mathbf{k}_{\|}$ on the boundary of the irreducible element of the two-dimensional first Brillouin zone. For the values of the parameters defining the surfaces each dispersion curve displays an absolute band

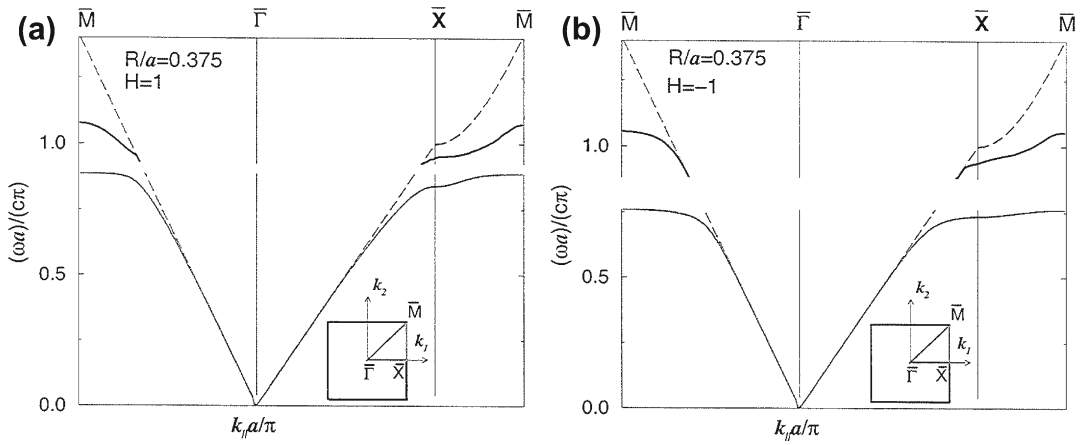

FIGURE 7.6

The dispersion curves for surface electromagnetic waves on a square lattice of hemiellipsoids on the planar surface of a perfect conductor in the non-radiative region of ω and $\mathbf{k}_{\|}$ values are plotted as functions of $\mathbf{k}_{\|}$ along the boundary of the irreducible element of the two-dimensional first Brillouin zone depicted in the insets. The values of the parameters assumed in obtaining these results are (a) $R/a = 0.375$, $H = 1$, $N_{max} = 10$; (b) $R/a = 0.375$, $H = -1$, $N_{max} = 10$.

gap within the non-radiative region of ω and $\mathbf{k}_{\parallel}$ values, with a second, higher frequency branch within the non-radiative region. For both the surface formed from protuberances and the surface formed from indentations the lowest frequency branch of the corresponding dispersion curves bends away from the vacuum light line into the non-radiative region as the boundary of the Brillouin zone is approached, more strongly in Fig. 7.6b than in Fig. 7.6a. Thus, the corresponding surface waves display the phenomenon of wave slowing.

7.3 Experimental Results

Experimental studies of surface electromagnetic waves on periodically structured perfectly conducting surfaces have been carried out on structured metal surfaces in the gigahertz and terahertz regions of the electromagnetic spectrum, where a metal is well represented by a perfect conductor. Experiments have been carried out on both one- and two-dimensional periodically structured surfaces. We consider the results for these two types of surfaces in turn.

7.3.1 One-Dimensional Surfaces

The propagation of microwave surface electromagnetic waves on a composite grating structure consisting of an alternating sequence of two rectangular grooves of different depths cut into a metal (copper) surface was studied theoretically and experimentally by Gao *et al.* [7.27]. The dispersion curve of this structure consists of two branches. The lower frequency branch is determined primarily by the single-period grating with the deep grooves; the higher frequency branch is determined primarily by the single-period grating with the shallow grooves. These two frequency bands can be varied independently by changing the depths of the two grooves from which the structure is constructed. The experimental results obtained are in good agreement with the calculated results.

Several of the experimental studies of surface electromagnetic waves on periodically structured surfaces have been devoted to the guiding of such waves by one-dimensional surface structures of various types.

The guiding of terahertz surface electromagnetic waves by a one-dimensional periodic array of rectangular holes on the surface of an aluminum film has been studied by THz time-domain spectroscopy [7.50]. The properties of the waves guided by this structure depend strongly on the length of the holes in the direction of propagation and on their depth. When the holes become sufficiently deep, they support electromagnetic resonances at discrete frequencies, which manifest themselves as peaks at the corresponding frequencies in the spectral dependence of the transmissivity of the structure. The lateral confinement of the guided wave decreases with increasing groove depth, and its propagation length increases to as much as 12 cm. In general, the measured mode properties proved to be larger than those calculated for a perfectly conducting structure. The long propagation length enabled the fabrication and characterization of a Y-splitter on the basis of this waveguide.

In a related study [7.51] these authors studied the effects of changing the geometrical parameters of the rectangular holes and the thickness of the film on the propagation of the guided waves they support. It was found to be possible to vary the number of propagating modes and their frequencies, as well as the lateral confinement of the modes and their propagation lengths in this manner.

The guiding of gigahertz surface electromagnetic waves by a one-dimensional periodic metallic structure that is the inverse of the one studied in Refs. [7.50,7.51] has been investigated by Zhao *et al.* [7.52]. The rectangular holes of finite depth employed in Refs. [7.50,7.51] were replaced by rectangular protuberances of finite height similar to the dominos studied theoretically for the guiding of surface waves on structured perfectly conducting surfaces in Ref. [7.53]. The electromagnetic field of the wave guided by this structure can be confined to an area of 0.04λ-by-0.3λ in the plane transverse to the direction of propagation, where λ is its wavelength in air. The mode size can be shrunk to $0.01\lambda_0$-by-$0.02\lambda_0$ in the THz region, where λ_0 is the wavelength in free space, by coating the structure with silicon.

An interesting type of guiding structure for surface waves in the microwave frequency range has been developed by Shen *et al.* [7.54]. These authors fabricated a thin (18 μm) copper strip one of whose edges was decorated with an array of rectangular grooves whose period was 5 mm. The copper strip was bonded to a single layer of polyimide (12.5 μm) by an epoxy adhesive (13 μm). The total thickness of this sample is 43.5 μm. It is therefore ultra thin and flexible,and can be wrapped around curved surfaces. The surface waves that propagate over curved surfaces were termed conformal surface plasmons. The structure supporting them can be designed to operate in the spectral range from the microwave to mid-infrared frequencies. A near-field scanning system was used to map the localized electromagnetic fields above the comb-shaped metal strip. The operating frequency was fixed at 10 GHz. The experimental results showed good confinement in both lateral directions and long propagation lengths of the conformal surface plasmons as they traveled on several curved surfaces, including sharp bends. These modes appear to be promising for use in a wide variety of plasmonic devices operating in a broad spectral range.

In concluding this section we note that surface plasmon polaritons exist not only at a dielectric-metal interface. They also exist at the interface between a dielectric and an *n*-type semiconductor. In Ref. [7.24] Li *et al.* have demonstrated the propagation of terahertz waves bound to an interface between air and a highly-doped silicon surface on which a one-dimensional periodic array of V-shaped grooves was fabricated.

7.3.2 Two-Dimensional Surfaces

Even before the current interest in surface electromagnetic waves on structured perfectly conducting surfaces arose, theoretical and experimental studies were being carried out for such waves in the microwave and terahertz wavelength regions, where a metal is well represented by a perfect conductor. In a notable study Sievenpiper *et al.* [7.35] investigated surface electromagnetic waves at microwave wavelengths on a structure consisting of a flat metal sheet on which a square lattice of mushroom-shaped protrusions is placed. The surface wave band structure of this surface was calculated by means of the finite element method for two-dimensional wave vectors along the edge of the irreducible element of the two-dimensional first Brillouin zone of the square lattice. It has the interesting feature that the dispersion curve of the lowest frequency branch, of TM or *p* polarization, follows the vacuum light line up to a certain frequency, where it suddenly becomes very flat. At a frequency slightly higher than the maximum frequency of this TM polarized branch a second branch, of TE or *s* polarization, begins, and continues upward with a slope smaller than the vacuum speed of light. The TM band does not reach the TE band edge, but stops below it, forming band gap. Higher frequency branches of the band structure are also obtained in these calculations. Thus, this structured surface supports surface electromagnetic waves

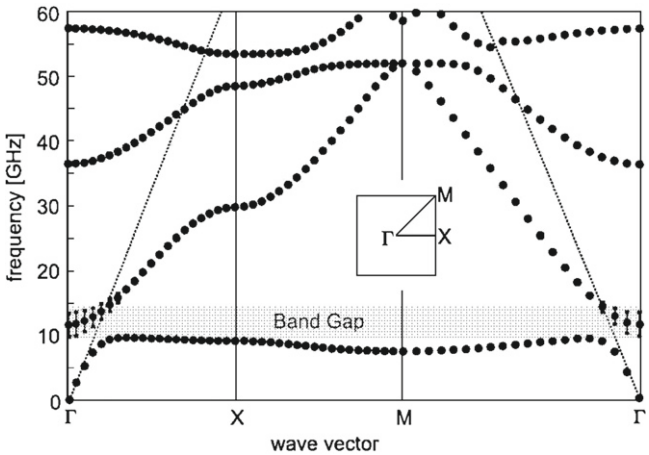

FIGURE 7.7

The dispersion curves for surface electromagnetic waves on a perfectly conducting surface patterned with a square lattice of mushroom-shaped protrusions in the non-radiative region of ω and $\mathbf{k}_{\parallel}$ along the boundary of the irreducible element of the two-dimensional first Brillouin zone depicted in the inset. The radiative broadening of the TE modes above the light line is indicated by error bars (Ref. [7.35]).

of both TM and TE polarizations, in non-overlapping frequency ranges, and displays an absolute band gap between the first and second branches. Experimental results obtained by these authors confirmed the results of their theoretical studies. The dispersion curve calculated by Sievenpiper *et al.*, and their experimental results are presented in Fig. 7.7.

In this and in subsequent experimental work the structures studied differed in most cases from those assumed in the theoretical studies of these surface electromagnetic waves. Nevertheless, the results obtained were in good agreement with the theoretical predictions.

In an experimental observation of surface electromagnetic waves localized to a structured metal surface in the gigahertz frequency region carried out by Hibbins *et al.* [7.55], the reflectivity of microwaves from a nearly perfectly conducting substrate perforated by holes was measured. Results of the theory presented in Ref. [7.4] were used to determine the structural parameters of a surface that would support a surface wave in this frequency region.

The structure studied in this work was a 300 mm $\times$ 300 mm array of hollow brass tubes of square cross section, length 45 mm, side length $d = 9.525$ mm, and inner length $a = 6.960$ mm. These tubes were arranged, square face down, on a flat brass plate and tightly clamped together. On the surface of the array of tubes was placed a periodic array of parallel brass cylindrical rods of radius $r = 1.0$ mm, with a period $2d$ (Fig. 7.8). These were introduced to control the strength of the diffractive coupling to the surface mode supported by the structure, which otherwise would be very weak.

Reflectivity spectra were measured for a series of fixed values of the polar angle of incidence θ. The incident field was p polarized with the xz plane as the plane of incidence, and only the p-polarized component of the specularly reflected field was registered. The surface mode was revealed as a dip in the frequency dependence of the reflectivity. A typical reflectivity spectrum, recorded at $\theta \cong 14°$ is

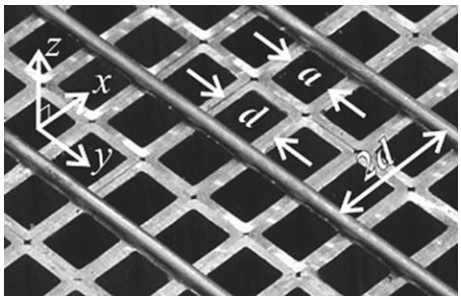

FIGURE 7.8

Photograph of the experimental sample showing the square brass tubes ($d = 9.525$ mm, $a = 6.960$ mm) and brass cylindrical rods (radius $r = 1.0$ mm). The coordinate system is also shown (Ref. [7.55]).

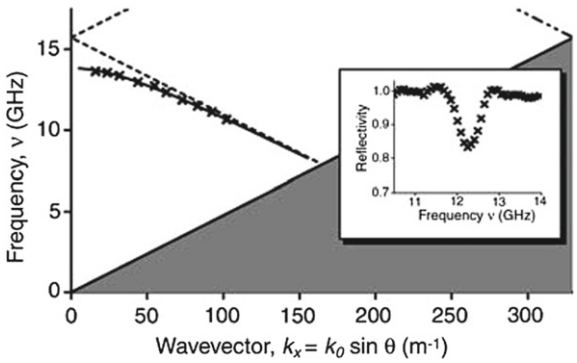

FIGURE 7.9

The dispersion of the surface mode on the air-filled sample. The plane of incidence is the *xz* plane. The frequency of the resonance is derived from experimental (*x*) and modeled (sold curve) data sets. The shaded region represents the region of the frequency-wavenumber plane within which surface modes cannot be directly coupled to, since they lie to the right of the vacuum light line. The dashed curves depict the first-order diffracted light lines centered on $k_x = \pm 2\pi/(2d) = \pm 300$ m^{-1} associated with the array of cylindrical rods. The dot-dashed curve similarly corresponds to first-order diffraction from the array of brass tubes. The inset shows the TM-polarized reflectivity spectrum obtained for an angle of incidence $\theta \sim 14°$, and illustrates the resonant surface mode at ~12.3 GHz (Ref. [7.55]).

presented in the inset to Fig. 7.9. With the use of the relation $k_x = (\omega/c)\sin\theta$, the dispersion curve for the surface mode was constructed from the results of a series of such measurements and is presented in the main part of Fig. 7.9. This dispersion curve lies on the second branch of the dispersion relation in the reduced zone scheme, and lies in the radiative region of the (ω, k_x) plane, to the left of the vacuum light line. This is why it can be excited by an incident volume electromagnetic wave. It is, therefore, strictly speaking a leaky surface wave. The experimental results are in very good agreement with results calculated with the finite element method.

In these experiments additional measurements were made when the tubes were filled with wax. Again, good agreement between the experimental and computational results was found.

In subsequent work Williams *et al.* [7.56] studied the guiding of surface plasmon polaritons in the terahertz frequency region on a copper surface patterned with a square array of annular holes of finite depth, each of which supports both a TEM coaxial mode and a TE_{11} coaxial mode. The dispersion curve of the surface modes supported by this structure consists of two branches, each of which can be varied independently of the other. The ability to guide two modes can be useful in waveguide-based chemical or biochemical sensing [7.57], where the ability to ratio responses in at least two frequency bands with high dynamic range is desirable for quantitative analysis. Terahertz time-domain spectroscopy was used to determine the decay lengths of the electric field of the surface modes into the vacuum, which were found to be of the order of 500 μm at frequencies of the order of 1 THz. This is about a factor of a hundred smaller than the decay length into the vacuum of a surface wave on a planar copper surface at such a frequency [7.58]. The amplitude mean free path of the surface mode along the surface was estimated from the data and the theory of Zenneck surface waves on copper [7.58] to be of the order of 5 cm at a frequency of about 1.45 THz.

Lockyear *et al.* [7.59] used the method of attenuated total reflection in the Otto geometry [7.60] to determine the dispersion curve of surface electromagnetic waves on a structured copper surface in the gigahertz frequency range. It consisted of square 18 μm thick copper patches of edge length 1.3 μm arranged in a square array with a period of 1.6 mm. The patches were separated from a copper ground plane by a low loss 0.79 mm thick dielectric layer. Each copper patch, however, was connected to the ground plane by a hollow copper via with a 0.15 mm radius. A p-polarized electromagnetic field was incident on the sample through a large wax prism at an angle of incidence greater than the critical angle for total internal reflection at the wax-air interface ($\theta_0 = 41.8°$, where θ_0 is the angle of incidence in the prism). The prism was placed above the sample at a variable distance t from it. The surface mode was observed as a strong reflectivity minimum in the frequency dependence of the specularly reflected beam. At each angle of incidence in the range $42° < \theta_{int} < 71°$ the distance t was varied in the range 3.5 mm $< t <$ 7.5 mm, allowing the optimum coupling condition to be found. For this optimum condition the resonant frequency of the mode was determined, which allowed the in-plane wave number $k_{\|}$ to be found, and the mode's dispersion curve constructed. In Fig. 7.10 is shown the dispersion of the surface mode at the optimum coupling condition for internal angles in the range $42° < \theta_{int} < 71°$. Also shown is a dispersion curve calculated by the finite element method.

The agreement between the two sets of results is very good. The inset to Fig. 7.10 shows a typical reflectivity spectrum for several values of the gap width t for an internal angle of incidence $\theta_{int} = 58.2°$. It is seen that changing the gap width brings the resonant coupling through an optimum condition ($t_{opt} = 5.5$ mm), and also shifts the resonance frequency. The latter effect is mainly due to the penetration of the exponentially decaying fields of the surface waves into the wax prism.

The work of Lockyear *et al.* demonstrates that it is possible to couple incident microwave radiation into a surface electromagnetic wave by means of the Otto ATR geometry. Moreover, the surface used in this study was significantly thinner than other surfaces used in this frequency region for such studies, much thinner than the operating wavelength. Finite element calculations also showed that the electromagnetic field in this mode is strongly localized to the surface.

In the experiments described up to now the tightly bound surface electromagnetic waves in the microwave and terahertz frequency regions were excited on the illuminated side of the structure

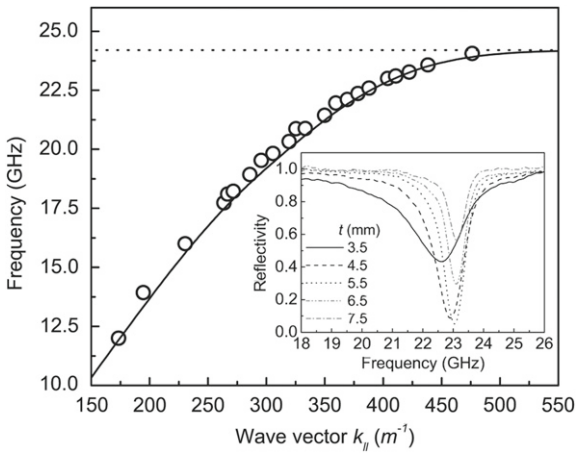

FIGURE 7.10

(circles) The dispersion of the TM-polarized surface mode supported by the sample compared to the predictions of the finite element method (solid curve). The frequency of the lower band edge associated with the sample, to which the dispersion curve is asymptotic, is depicted by the dotted line. The inset shows the specular reflection from the sample as a function of frequency for $\theta_{int} = 58.2°$. Here the width of the air gap t is varied between 3.5 and 7.5 mm in 1 mm steps. The resulting shift in the resonant frequency is attributed to field penetration into the wax prism, due to the latter's close proximity to the sample surface. Note the optimum coupling condition at $t_{opt} = 5.5$ mm (Ref. [7.59]).

supporting them. Kushiyama *et al.* [7.61] predicted a slab structure that allows the excitation of these surface waves on the back surface of the slab in the Kretschmann attenuated total reflection configuration [7.62]. This configuration is convenient for applications such as sensing devices. The structure consists of a three-dimensional metallic wire mesh in which a metallic sphere is added to the center of each of its links. In an experimental study of this structure the excitation of the surface electromagnetic wave was revealed as a dip in the frequency dependence of the reflectivity for a fixed angle of incidence.

7.4 Conclusions

The results of the calculations and measurements described in this chapter show that a one- or two-dimensional periodically structured perfectly conducting surface can bind a surface electromagnetic wave to it. The dispersion curves of these surface waves can be varied in desirable ways by changing the parameters defining the surfaces: the widths, depths, and shapes of their indentations, the material they are filled with, and the period of the structure. They are therefore more easily manipulated than are the dispersion curves of surface plasmon polaritons at planar dielectric-metal interfaces. An important consequence of this capability is that it is now possible to create devices based on surface electromagnetic waves for applications in the microwave or terahertz ranges, where surface plasmon polaritons on planar surfaces cannot be used. Examples include the study of electronic coherence in semiconductors [7.63],

pharmaceutical quality control [7.64], in chemical and biochemical sensing [7.57], and in security screening [7.65]. Several of these applications will be discussed in detail in other chapters of this book.

Acknowledgments

I would like to acknowledge support from Air Force Research Laboratory Contract FA 9453–08-C-0230. I thank Dr. S. Chakrabarti for preparing Figs. 7.1 and 7.2, Dr. E. I. Chaikina for preparing Figs. 7.3 and 7.5, Professor F. J. García-Vidal for providing Fig. 7.4, Professor I. Simonsen for providing Fig. 7.6, Professor D. Sievenpiper for providing Fig. 7.7, and Professor J. R. Sambles for providing Figs. 7.8–7.10. I am grateful to Professor Sambles for a critical reading of the manuscript.

References

[7.1] Goubau, G. (1950). Surface waves and their application to transmission lines. *J. Appl. Phys.* **21**, 1119–1128.
[7.2] Rotman, W. (1951). A study of single-surface corrugated guides. *Proc. IRE* **39**, 952–959.
[7.3] Mills, D. L., and Maradudin, A. A. (1989). Surface corrugation and surface-polariton binding in the infrared frequency range. *Phys. Rev. B* **39**, 1569–1574.
[7.4] Pendry, J. B., Martín-Moreno, L., and García-Vidal, F. J. (2004). Mimicking surface plasmons with structured surfaces. *Science* **305**, 847–848.
[7.5] García-Vidal, F. J., Martín-Moreno, L., and Pendry, J. B. (2005). Surfaces with holes in them: new plasmonic metamaterials. *J. Opt. A, Pure Appl. Opt.* **7**, S97–S101.
[7.6] Maier, S. A., Andrews, S. R., Martín-Moreno, L., and García-Vidal, F. J. (2006). Terahertz surface plasmon-polariton propagation and focusing on periodically corrugated metal wires. *Phys. Rev. Lett.* **97**, 176805 (1–4).
[7.7] Chen, Y., Song, Z., Li, Y., Hu, M., Xing, Q., Chang, Z., Choi, L., and Wang, C.-Y. (2006). Effective surface plasmon polaritons on the metal wire with arrays of subwavelength grooves. *Opt. Express* **14**, 13021–13029.
[7.8] Fernández-Dominguez, A. I., Williams, C. R., Martín-Moreno, L., García-Vidal, F. J., Andrews, S. R., and Maier, S. A. (2008). Terahertz surface plasmon polaritons on a helically grooved wire. *Appl. Phys. Lett.* **93**, 141109 (1–3).
[7.9] Fernández-Dominguez, A. I., Moreno, E., Martín-Moreno, L., and García-Vidal, F. J. (2009). Guiding terahertz waves along subwavelength channels. *Phys. Rev. B* **79**, 233104 (1–4).
[7.10] Fernández-Dominguez, A. I., Moreno, E., Martín-Moreno, L., and García-Vidal, F. J. (2009). Terahertz wedge plasmon polaritons. *Opt. Lett.* **34**, 2063–2065.
[7.11] Fernández-Dominguez, A. I., Williams, C. R., García-Vidal, F. J., and Martín-Moreno, L. (2011). Surface electromagnetic waves on structured perfectly conducting surfaces, *in* "Structured Surfaces as Optical Metamaterials," (A. A. Maradudin Ed.) pp. 232–268 Cambridge University Press, Cambridge, UK.
[7.12] Bulgakov, A. A., and Khankina, S. I. (1982). Quasi-steady state surface acoustic waves at a rough solid surface. *Solid State Commun.* **44**, 55–57.
[7.13] Huang, X., and Maradudin, A. A. (1987). Propagation of surface acoustic waves across random gratings. *Phys. Rev. B* **36**, 7828–7839.
[7.14] Kosachev, V. V., and Shchegrov, A. V. (1995). Dispersion and attenuation of surface acoustic waves of various polarizations on a stress-free randomly rough surface of a solid. *Ann. Phys. (NY)* **240**, 225–265.
[7.15] Leskova, T. A., Maradudin, A. A., and Simonsen, I. (2008). Surface electromagnetic waves on two-dimensional rough perfectly conducting surfaces. *Revista Mexicana de Física S* **54**, 54–65.

[7.16] Auld, B. A., Gagnepain, J. J., and Tan, M. (1978). Horizontal shear surface waves on corrugated surfaces. *Electronics Lett.* **12**, 650–652.
[7.17] Gulyaev Yu, V., and Plesskii, V. P. (1978). Slow, shear surface acoustic waves in a slow-wave structure on a solid surface. *Sov. Phys. Tech. Phys.* **23**, 266–269.
[7.18] Baghai-Wadji, A. R., and Maradudin, A. A. (1991). Shear horizontal surface acoustic waves on large amplitude gratings. *Appl. Phys. Lett.* **59**, 1841–1843.
[7.19] Shen, L., Chen, X., and Yang, T.-J. (2008). Terahertz surface plasmon polaritons on periodically corrugated metal surfaces. *Opt. Express* **16**, 3326–3333.
[7.20] Wang, B., Liu, L., and He, S. (2008). Propagation loss of terahertz surface plasmon polaritons on a periodically structured Ag surface. *J. Appl. Phys.* **104**, 103531 (1–6).
[7.21] Jiang, T., Shen, L., Zhang, X., and Ran, L. (2009). High-order modes of spoof surface plasmon polariton on periodically corrugated metal surfaces. *Progr. Electromagn. Res. M* **8**, 91–102.
[7.22] Glass, N. E., and Maradudin, A. A. (1981). Shear surface elastic waves on large amplitude gratings. *Electron. Lett.* **17**, 773–774.
[7.23] Maradudin, A. A., and Zierau, W. (1994). Surface acoustic waves of sagittal and shear horizontal polarization on large-amplitude gratings. *Geophys. J. Int.* **118**, 325–332.
[7.24] Li, S., Jadidi, M. M., Murphy, T. E., and Kumar, G. (2013). Terahertz surface plasmon polaritons on a semiconductor surface structured with periodic V-grooves. *Opt. Express* **21**, 7041–7049.
[7.25] Ruan, Z., and Qiu, M. (2007). Slow electromagnetic wave guided in sub wavelength region along one-dimensional periodically structured surface. *Appl. Phys. Lett.* **90**, 201906 (1–3).
[7.26] Zhang, X., Shen, L., and Ran, L. (2009). Low-frequency surface plasmon polaritons propagating along a metal film with periodic cut-through slits in symmetric or asymmetric environments. *J. Appl. Phys.* **105**, 013704 (1–7).
[7.27] Gao, X., Shi, J. H., Ma, H. F., Jiang, W. X., and Cui, T. J. (2012). Dual-band spoof surface plasmon polaritons based on composite-periodic gratings. *J. Phys. D: Appl. Phys.* **45**, 505104 (1–5).
[7.28] López-Rios, T., Mendoza, D., García-Vidal, F. J., Sánchez-Dehesa, J., and Pannetier, B. (1998). Surface shape resonances in lamellar metallic gratings. *Phys. Rev. Lett.* **81**, 665–668.
[7.29] Qiu, M. (2005). Photonic band structures for surface waves on structured metal surfaces. *Opt. Express* **13**, 7583–7588.
[7.30] Maier, S. A., and Andrews, S. R. (2006). Terahertz pulse propagation using plasmon-polariton-like surface modes on structured conductive surfaces. *Appl. Phys. Lett.* **88**, 251120 (1–3).
[7.31] Lan, Y. C., and Chern, R.-L. (2006). Surface plasmon-like modes on structured perfectly conducting surfaces. *Opt. Express* **14**, 11339–11347.
[7.32] Hendry, E., Hibbins, A., and Sambles, J. R. (2008). Importance of diffraction in determining the dispersion of designer surface plasmons. *Phys. Rev. B* **78**, 235426 (1–10).
[7.33] Garcia de Abajo, F. J., and Saenz, J. J. (2005). Electromagnetic surface modes in structured perfect-conductor surfaces. *Phys. Rev. Lett.* **95**, 233901 (1–4).
[7.34] Navarro-Cía, M., Beruete, M., Agrafiotis, S., Falcone, F., Sorolla, M., and Maier, S. A. (2009). Broadband spoof plasmons and subwavelength electromagnetic energy confinement on ultra thin metal films. *Opt. Express* **17**, 18184–18195.
[7.35] Sievenpiper, D., Zhang, L., Jimenez Broas, R. F., Alexopoulos, N. G., and Yablonovitch, E. (1999). High-impedance electromagnetic surfaces with a forbidden frequency band. *IEEE Trans. Microwave Theory Tech.* **47,** 2-59-2074.
[7.36] Chen, C.-C. (1970). Transmission through a conducting screen perforated periodically with apertures. *IEEE Trans. Microwave Theory Tech.* **18**, 627–632.
[7.37] Chen, C.-C. (1971). Diffraction of electromagnetic waves by a conducting screen perforated periodically with circular holes. *EEE Trans. Microwave Theory Tech.* **19**, 475–481.

[7.38] Chen, C.-C. (1973). Transmission of microwaves through perforated flat plates of finite thickness. *IEEE Trans. Microwave Theory Tech.* **21**, 1–6.
[7.39] Bliek, P. J., Botten, L. C., Deleuil, R., McPhedran, R. C., and Maystre, D. (1980). Inductive grids in the region of diffraction anomalies: theory, experiment, and application. *IEEE Trans. Microwave Theory Tech.* **22**, 1119–1125.
[7.40] Jackson, J. D. (1975). "Classical Electrodynamics." 2nd ed. Sections 8.2–8.4. John Wiley and Sons, New York.
[7.41] Rayleigh, Lord (1896). "The Theory of Sound." 2nd ed., vol. II, pp. 89, 297–311. MacMillan, London.
[7.42] Petit, R., and Cadilhac, M. (1966). Sur la diffraction d'une onde plane par un réseau infiniment conducteur. *C. R. Acad. Sci. B* **262**, 468–471.
[7.43] Millar, R. F. (1969). On the Rayleigh assumption in scattering by a periodic surface. *Proc. Camb. Philos. Soc.* **65**, 773–791.
[7.44] Hill, N. R., and Celli, V. (1978). Limits of convergence of the Rayleigh method for surface scattering. *Phys. Rev. B* **17**, 2478–2481.
[7.45] van den Berg, P. M., and Fokkema, J. T. (1979). The Rayleigh hypothesis in the theory of reflection by a grating. *J. Opt. Soc. Am.* **69**, 27–31.
[7.46] van den Berg, P. M., and Fokkema, J. T. (1980). The Rayleigh hypothesis in the theory of diffraction by a perturbation in a plane surface. *Radio Sci.* **15**, 723–732.
[7.47] Schlup, W. A. (1984). On the convergence of the Rayleigh ansatz for hard-wall scattering on arbitrary periodic surface profiles. *J. Phys. A: Math. Gen.* **17**, 2607–2619.
[7.48] DeSanto, J. A. (1981). Scattering from a perfectly reflecting arbitrary periodic surface: an exact theory. *Radio Sci.* **16**, 1315–1326.
[7.49] Paulick, T. C. (1990). Applicability of the Rayleigh hypothesis to real materials. *Phys. Rev. B* **42**, 2801–2824.
[7.50] Kumar, G., Pandey, S., Cui, A., and Nahata, A. (2011). Planar plasmonic terahertz waveguides based on periodically corrugated metal films. *New J. Phys.* **13**, 033024 (1–13).
[7.51] Zhu, W., Agrawal, A., Cui, A., Kumar, G., and Nahata, A. (2011). Engineering the propagation properties of planar plasmonic terahertz waveguides. *IEEE J, Sel. Top. Quant. Electron.* **17**, 146–153.
[7.52] Zhao, W., Eldaiki, O. M., Yang, R., and Lu, Z. (2010). Deep sub wavelength wave guiding and focusing based on designer surface plasmons. *Opt. Express* **18**, 21498–21502.
[7.53] Martin-Cano, D., Nesterov, M. L., Fernández-Domínguez, A. I., García-Vidal, F. J., Martín–Moreno, L., and Moreno, E. (2010). Domino plasmons for subwavelength terahertz circuitry. *Opt. Express* **18**, 754–764.
[7.54] Shen, X., Cui, T. J., Martin-Cano, D., and García-Vidal, F. J. (2013). Conformal surface plasmons propagating on ultrathin and flexible films. *Proc. Nat. Acad. Sci.* **110**, 40–45.
[7.55] Hibbins, A. P., Evans, B. R., and Sambles, J. R. (2005). Experimental verification of designer surface plasmons. *Science* **308**, 670–672.
[7.56] Williams, C. R., Misra, M., Andrews, S. R., Maier, S. A., Carretero-Palacios, S., Rodrigo, S. G., García-Vidal, F. J., and Martín-Moreno, L. (2010). Dual band terahertz waveguiding on a planar metal surface patterned with annular holes. *Appl. Phys. Lett.* **96**, 011101 (1–3).
[7.57] Nagel, M., Haring Bolivar, P., Brucherseifer, M., and Jurz, H. (2002). Integrated THz technology for label-free genetic diagnostics. *Appl. Phys. Lett.* **80**, 154–156.
[7.58] Jeon, T.-I., and Grischkowsky, D. (2006). THz Zenneck surface wave (THz surface plasmon) propagation on a metal sheet. *Appl. Phys. Lett.* **88**, 061113 (1–3).
[7.59] Lockyear, M. J., Hibbins, A. P., and Sambles, J. R. (2009). Microwave surface-plasmon-like modes on thin metamaterials. *Phys. Rev. Lett.* **102**, 073901 (1–4).

[7.60] Otto, A. (1968). Excitation of non radiative surface waves in silver by the method of frustrated total reflection. *Z. Phys.* **216**, 392–410.
[7.61] Kushiyama, Y., Arima, T., and Uno, T. (2012). Experimental verification of spoof surface plasmons in wire metamaterials. *Opt. Express* **16**, 18238–18247.
[7.62] Kretschmann, E., and Raether, H. (1968). Radiative decay of non radiative surface plasmons excited by light. *Z. Naturforsch. A* **23**, 2135–2136.
[7.63] Shah, J. (1996). "Ultrafast Spectroscopy of Semiconductors and Semiconductor Nanostructures.". Springer, New York.
[7.64] Strachan, C. J., Taday, P. F., Newnham, D. A., Gordon, K. C., Zeitler, J. A., Pepper, M., and Rader, T. (2005). Using terahertz pulsed spectroscopy to quantify pharmaceutical polymorphism and crystallinity. *J. Pharm. Sci.* **94**, 837–846.
[7.65] Yamamoto, K., Yamaguchi, M., Miyamaru, F., Tani, M., Hangyo, M., Ikeda, T., Matsushita, A., Koide, K., Tatsumo, M., and Minami, Y. (2004). Noninvasive inspection of C-4 explosive in mails by terahertz time-domain spectroscopy. *Jpn. J. Appl. Phys.* **43**, L414–L417.